2017-09-15

The onset of fabric development in deep marine sediments

Maffione, M

10.1016/j.epsl.2017.06.018
Earth and Planetary Science Letters
Elsevier BV

Maffione, M. and Morris, A., 2017. The onset of fabric development in deep marine sediments. *Earth and Planetary Science Letters*, **474**, 32-39, doi: 10.1016/j.epsl.2017.06.018.

The final version of this paper is available at:
http://www.sciencedirect.com/science/article/pii/S0012821X1730328X

The onset of fabric development in deep marine sediments

Marco Maffione[1,2] and Antony Morris[3]

[1]School of Geography, Earth and Environmental Sciences, University of Birmingham, Edgbaston, Birmingham, B15 2TT, UK

[2]Department of Earth Sciences, Utrecht University, Heidelberglaan 2, 3584 CS Utrecht, Netherlands

[3]School of Geography, Earth and Environmental Sciences, Plymouth University, Drake Circus, Plymouth, PL4 8AA, UK

Keywords

Sedimentary fabric; deep marine; compaction; magnetic anisotropy; AMS; International Ocean Discovery Program

Abstract

Post-depositional compaction is a key stage in the formation of sedimentary rocks that results in porosity reduction, grain realignment and the production of sedimentary fabrics. The progressive time-depth evolution of the onset of fabric development in deep marine sediments is poorly constrained due to the limited quantity and resolution of existing data. Here we present high-resolution anisotropy of magnetic susceptibility (AMS) results from clay-rich deep marine sediments recovered at International Ocean Discovery Program Site U1438 (Philippine Sea). AMS is a petrofabric tool sensitive to the preferred orientation of grains in rocks. Down-section variations of AMS parameters, density, porosity

and the inclination of magnetic remanences demonstrate that fabrics develop in response to compaction and dewatering but also that they do not develop progressively with depth below the mudline. Instead, a horizontal foliation first forms at 83 mbsf once the sediment load reaches an effective stress threshold for the onset of compaction and is then continuously enhanced down to 113 mbsf, defining a 30 m-thick 'initial compaction window'. The magnetostratigraphic age model for IODP Site U1438 indicates a delay of 5.7 Ma in initial fabric formation following sediment deposition, with strongly defined fabrics then taking an additional 6.5 Ma to develop.

1. Introduction

During deposition of (hemi)pelagic sediments in deep-sea environments, platy minerals (mainly phyllosilicates) tend to align with their long axes parallel to the water-sediment interface. Bottom-current disturbance and bioturbation, together with the natural predisposition of clay flakes to form edge-to-edge and edge-to-face contacts due to surface electric charge distribution (Bennett et al., 1991), eventually result in an uppermost sedimentary interval characterized by a chaotic internal structure (i.e., isotropic fabric) and high porosity and water content (Bennett et al., 1991; Reynolds and Gorsline, 1992). With increasing vertical burial load at depth, clays particles rotate to form horizontal face-to-face contacts, accompanied by simultaneous dewatering and porosity reduction (Bennett et al., 1981; Bennett and Hulbert, 1986). The effect of this process on the microstructure of the sediment is the formation of a fabric characterized by a well-defined horizontal foliation plane.

The majority of dewatering and compaction in pelagic sedimentary sequences is thought to occur progressively within the uppermost stratigraphic intervals (e.g., Arason and Levi, 1990). However, only a few previous studies have investigated microstructure changes during compaction and initial fabric development in deep marine environments (Kopf and Behrmann, 1997; Hirano et al., 2001; Kawamura and Ogawa, 2002; 2004), and none have a sufficiently high spatial and temporal resolution to describe in detail the evolution of this process. Here we present results of a high-resolution anisotropy of magnetic susceptibility (AMS) analysis of a sequence of unconsolidated deep marine sediments recovered in the Philippine Sea by International Ocean Discovery Program (IODP) Expedition 351 (Arculus et al., 2015a), where magnetostratigraphy provides an accurate age model. We use AMS as a sensitive measure of fabric development in these sediments (e.g., Rochette et al., 1992; Tarling and Hrouda, 1993; Borradaile and Jackson, 2004), and compare magnetic fabric parameters with other physical properties to tightly constrain the depth and timing of the onset and evolution of fabric development in a deep marine environment.

2. Geological background and sampling

2.1. Tectonic framework of the Philippine Sea Plate and IODP Site U1438

The Philippine Sea Plate (PSP) is an oceanic plate located between the Eurasia and Pacific plates and bordered by active subduction zones (Figure 1). The PSP can be subdivided into three tectono-stratigraphic domains: (i) a western domain floored by a complex array of oceanic plateaux, ridges, and basins of Cretaceous to Oligocene age and bordered to the east by the Eo-Oligocene (~55-

25 Ma) Kyushu-Palau Ridge (e.g., Deschamps and Lallemand, 2003; Okino and Fuijoka, 2003; Ishizuka et al., 2011a, 2013); (ii) a central domain dominated by the Miocene (~25-12 Ma) Parece Vela-Shikoku back-arc basin (Okino et al., 1994) occurring between the Kyushu-Palau Ridge and the modern Izu-Bonin-Mariana (IBM) arc; and (iii) an eastern domain forming the forearc region between the modern IBM arc and the IBM trench, developed upon initiation of subduction of the Pacific plate below the PSP at ~52 Ma (Ishizuka et al., 2011b; Reagan et al., 2010; Arculus et al., 2015b).

During June and July 2014, IODP Expedition 351 (Arculus et al., 2015a) recovered a suite of sedimentary and volcanic rocks at Site U1438 (4700 m water depth) in the western domain of the PSP (Amami Sankaku Basin; 27.38°N, 134.32°E; Figure 1a). Four progressively deeper holes were drilled at this site, down to 26.5, 257.3, 897.8, and 1611 metres below seafloor (mbsf), at Holes U1438A, B, D and E respectively. Recovered rocks (Figure 1b) consist of a thick sedimentary sequence (Units I-IV) deposited since the Early Eocene (~55 Ma) and recording the birth, evolution and death of the Kyushu-Palau Ridge, overlying igneous basement rocks (Unit 1).

2.2. Deep marine sedimentation in the west PSP (Unit I)

Unit I (0-160.3 mbsf; Hole U1438B) is an unconsolidated fine-grained pelagic and hemipelagic sedimentary sequence composed of mud, tuffaceous mud, mud with ash, and clay with discrete ash beds. Paleomagnetic and biostratigraphic constraints place the base of Unit I at the Miocene-Oligocene transition (Arculus et al., 2015a). Deposition of Unit I therefore started soon after the demise of Kyushu-Palau Ridge volcanism and initial opening of the Parece Vela-Shikoku

back-arc basin to the east (thought to occur at ~25 Ma; Okino et al., 1994). Since no significant tectonic events occurred since that time at the location of Site U1438, Unit I represents the product of deep marine sedimentation, with sedimentation rates ranging from ~2 to ~0.5 cm/kyr (Arculus et al., 2015a). The average grain size of Unit I changes slightly down-core, with the uppermost interval (0-45 mbsf) mainly represented by siltstones with a significant (up to 60%) biogenic, mainly siliceous component, a central interval (45-93 mbsf) dominated by claystones with a lower biogenic content, and a bottom interval (93-160.3 mbsf) represented again predominantly by siltstones. Bioturbation is rare in the upper interval of Unit I (< 93 mbsf) and increases at depth, with more bioturbated intervals occurring below 121 mbsf. X-Ray diffraction analyses revealed a predominant assemblage of quartz, plagioclase, chlorite, muscovite, illite and other clay minerals (Arculus et al., 2015a). Below ~93 mbsf (in the lower siltstones) quartz content decreases, while the content of zeolite and clay minerals increases.

3. Methods

Anisotropy of magnetic susceptibility (AMS) is a petrofabric tool used to determine the preferred orientation of minerals (e.g., Jelínek, 1981; Hrouda, 1982; Borradaile, 1988; Rochette et al., 1992; Tarling and Hrouda, 1993; Borradaile and Jackson, 2004). AMS is geometrically described by an ellipsoid with principal axes corresponding to the minimum (k_{min}), intermediate (k_{int}), and maximum (k_{max}) susceptibilities (Hrouda, 1982). The relative magnitude of the susceptibility axes defines the shape of the AMS ellipsoid, which can be: (1) isotropic ($k_{min} = k_{int} = k_{max}$) when grains are not aligned preferentially; (2) oblate

($k_{min} << k_{int} \approx k_{max}$) when grain alignment defines a foliation plane; (3) triaxial ($k_{min} < k_{int} < k_{max}$) when grain alignment results in a well-defined foliation and a lineation; or (4) prolate ($k_{min} \approx k_{int} << k_{max}$) when grain alignment defines a lineation. Here we describe the strength of anisotropy using the corrected anisotropy degree (P_J; Jelínek,1978), where $P_J = 1.0$ indicates an isotropic fabric and, e.g., $P_J = 1.05$ indicates 5% anisotropy. The shape of the ellipsoid is described by the shape parameter (T), where $-1.0 < T < 1.0$ and positive/negative values of T indicate oblate/prolate fabrics respectively (Jelínek 1978). Sedimentary fabrics are characterised by $P_J > 1.0$, oblate AMS ellipsoids ($0 < T < 1$), vertical k_{min} axes, and k_{int} and k_{max} axes dispersed within the horizontal foliation plane.

We measured the anisotropy of low-field magnetic susceptibility of 173 discrete, 8 cm^3 cubic samples from the top 140 m of Unit I. Measurements were carried out using an AGICO KLY-3S Kappabridge (Plymouth University), and susceptibility tensors and associated eigenvectors and eigenvalues calculated using AGICO Anisoft 4.2 software. Instrument precision for AMS measurements for the KLY-3S system is > 99%, yielding meaningful principal directions in weakly anisotropic rocks when $P_J > 1.003$ (Burmeister et al., 2009). Sample orientations were determined by correcting cores recovered from Hole U1438B to the geographic reference frame using "FlexIT" tool data obtained during advanced piston corer (APC) deployments (Arculus et al., 2015a).

Rock magnetic experiments were performed to investigate the nature of the mineral fractions contributing to the AMS. Curie temperatures were determined from the high-temperature (20-700°C) variation of magnetic susceptibility of representative samples, measured using a KLY-3S coupled with a CS-3 high-

149 temperature furnace apparatus. Isothermal remanent magnetization (IRM)
150 acquisition experiments were conducted on representative samples using a
151 Molspin pulse magnetizer to apply peak fields up to 800 mT with resulting IRMs
152 measured using an AGICO JR6A spinner magnetometer.
153 Finally, we also employ shipboard paleomagnetic and physical property data
154 from Hole U1438B, collected using methods documented in Arculus et al.
155 (2015a).
156
157 **4. Results**
158 AMS parameters from the investigated interval of Unit I are extremely variable
159 with depth, with a clear change occurring at 83 mbsf (Figure 2; Supplementary
160 material Table 1). The anisotropy degree is low (P_J ≈1.006) indicating weakly
161 anisotropic sediments in the uppermost 83 m of the sequence, but progressively
162 increases over an interval of ~30 m below 83 mbsf, reaching a maximum of P_J
163 ≈1.060 at 113 mbsf (Figure 2a). Similarly the shape parameter (T) is extremely
164 variable from -1.0 to +1.0 in the upper interval, becoming consistently oblate
165 (0.6 < T < 1.0) immediately below 83 mbsf, and then strongly oblate (0.8 < T <
166 1.0) below 113 mbsf (Figure 2b). In addition, the orientation of the principal
167 susceptibility axes changes with depth. Above 83 mbsf, magnetic fabrics are
168 randomly oriented, with only the k_{min} axes showing a faint alignment near the
169 vertical (Figure 3a). Below 83 mbsf, k_{min} axes become tightly clustered along the
170 vertical, and the k_{int} and k_{max} axes align with the horizontal plane (Figure 3b). A
171 weak clustering of k_{max} axes along an ESE-NWN orientation is also observed,
172 potentially reflecting weak bottom water currents during deposition (Hrouda

and Jezek, 1999). Mean magnetic susceptibility shows a slight increase with depth from ~30 to ~80 x 10^{-5} SI (Figure 2c).

Results from high-temperature variation of magnetic susceptibility experiments revealed consistent maximum Curie temperatures of ~580°C (Figure 4a), indicating that the ferromagnetic fraction in these sediments is dominated by near-stoichiometric magnetite (Dunlop and Özdemir, 1997). This is consistent with IRM acquisition experiments, where saturation was reached at applied fields of 200-300 mT (Figure 4b), consistent with the presence of low-coercivity, fine-grained (single-domain to pseudo-single-domain) magnetite. However, the vertical alignment of k_{min} axes (perpendicular to horizontal bedding in the sediments) indicates a dominance of normal sedimentary fabrics, and excludes the presence of significant inverse magnetic fabric components due to single domain effects in these sediments (Potter and Stephenson, 1988).

5. Discussion

5.1. Comparison of AMS fabric variations with physical properties

Interpretation of AMS data requires understanding of the source of the susceptibility signal and its potential variability downhole. A linear relationship between low field magnetic susceptibility and the intensity of natural remanent magnetization (NRM) suggests constancy of ferromagnetic mineralogy and grain-size (domain state) through Unit I (Figure 4c), implying that the contribution of magnetite to the susceptibility signal is controlled by concentration alone. The relatively low bulk magnetic susceptibility (Figure 2c), however, indicates that magnetite content is low and that the paramagnetic phyllosilicate matrix is likely the main contributor to susceptibility in these

198 sediments, as typically observed in clay-rich sediments (e.g., Borradaile and
199 Jackson, 2004; Sagnotti and Speranza, 1993; Maffione et al., 2012, 2015; Parés,
200 2015).
201 The rapid increase of the anisotropy degree, together with the acquisition of a
202 consistently oblate fabric below 83 mbsf within Unit I (Figure 2) marks the onset
203 of development of a horizontal foliation typical of sedimentary fabrics (Figure
204 3b). This foliation is progressively enhanced down to 113 mbsf, where the
205 anisotropy degree reaches a maximum and AMS ellipsoids become strongly
206 oblate (Figure 2b). This depth interval of fabric development coincides with a
207 distinct decrease in porosity from 75 to 65% and increase in bulk density from
208 ~1.45 to ~1.55 g/cm^3 (Figure 2d), seen in shipboard physical property data
209 acquired on discrete samples analysed during IODP Expedition 351 (Arculus et
210 al., 2015a). This suggests that fabrics have developed in response to mechanical
211 compaction and dewatering occurring during burial diagenesis due to increasing
212 effective overburden stress. Chemical compaction is considered insignificant in
213 Unit I, as this generally only becomes a significant porosity-occluding process at
214 depths greater than ~2 km (Bjørlykke and Høeg, 1997; Mondol et al., 2008). An
215 apparent increase in sedimentation rate from ~0.5 to ~2.0 cm/ka at 83 mbsf
216 (Figure 2e) is likely to also result from mechanical compaction rather than a
217 change in rate of sediment supply.
218
219 *5.2. Paleomagnetic evidence for compaction*
220 As an additional test for the compaction-related origin of fabric development we
221 analyzed the occurrence of inclination shallowing of paleomagnetic remanences,
222 which characteristically results from compaction (e.g., Anson and Kodama, 1987;

223 Arason and Levi, 1990; Tauxe and Kent, 2004; Huang et al., 2013). Shipboard
224 remanence directions are presented in Figure 5 (based on measurements of
225 archive half core sections following alternating field demagnetization at 25 mT to
226 remove significant drilling-induced components; Figure 6). Inclinations above 83
227 mbsf are close to the value expected at IODP Site U1438, but are generally
228 shallower than expected below this (Figure 5a). To test this statistically, we
229 selected only data from the bottom 1.0 m of each core in order to exclude
230 intervals affected by drilling-induced shearing (commonly encountered in IODP
231 piston cores (Acton et al., 2002) and evident in the declination data of Figure 5b).
232 Mean inclinations were calculated after transposing all data to normal polarity
233 and applying a fixed 45° cut-off to the distribution of corresponding virtual
234 geomagnetic poles (following the methodology of Johnson et al. (2008)). For the
235 uppermost 83 m of Unit I, the mean inclination of 44.1° (α_{95} = 1.2°, n = 408) is
236 not statistically different from the expected geocentric axial dipole (GAD)
237 inclination at this site (I = 46°). In contrast, the mean inclination below 83 mbsf
238 (I = 39.7°; α_{95} = 1.8°, n = 266) is statistically significantly shallower. Using the
239 elongation/inclination (E/I) correction method (Tauxe and Kent, 2004) we
240 obtained an unflattened inclination for the interval 83-140 mbsf of 42.8° (95%
241 confidence limits: 40.2°-53.4°) consistent with the expected inclination. These
242 results further confirm that mechanical compaction has affected the lower
243 interval of Unit I but is absent or not statistically significant at shallower depths.
244
245 *5.3. Potential causes of the sudden onset of fabric development at 83 mbsf*
246 *5.3.1. Comparison with compaction trends for marine mudrocks*

247 Effective stress-controlled mechanical compaction at the relative shallow depths
248 of Unit I in Hole U1438B might be expected to produce continuous changes in
249 physical properties, i.e. with a progressive decrease in porosity and increase in
250 anisotropy degree with depth. Following Kopf and Behrmann (1997), we
251 compare downhole porosity variations with published mechanical compaction
252 functions by converting porosity determinations to uniaxial vertical shortening
253 values, e_v using:

$$e_v = \frac{P_0 - P}{P - 100}$$

254 where P is a given sample porosity (in %) and P_0 is an initial porosity near the
255 mudline (taken as 75%). Figure 7 compares the resulting values to converted
256 porosity-depth trends for clays and claystones of Terzaghi (1925), Athy (1930),
257 Hamilton (1976) and Sclater and Christie (1980). Though variable, each model
258 predicts a smooth, monotonic increase in shortening with depth, in contrast to
259 the stepwise increase at 83 mbsf in Unit I from e_v values close to zero (mean = -
260 0.03) to a mean value of -0.21 below. This is consistent with the AMS data that
261 show a uniformly low anisotropy degree down to 83 mbsf and then a sharp
262 change in character to pronouncedly oblate fabrics. Hence, factors other than
263 continuous compaction across the whole depth interval of Unit I must influence
264 fabric development in these sediments.
265
266 *5.3.2. Apparent overconsolidation*
267 The sharp increase of the anisotropy degree in the studied unit resembles the
268 pattern expected for "apparent overconsolidation" (Schwehr et al., 2006),
269 whereby sediments appear more consolidated than predicted by simple burial

for a given depth. According to Schwehr et al. (2006) apparent overconsolidation can result from unconformities produced by underwater landslides, which unload pre-consolidated sediments that then become buried by new sediments. Alternatively, overconsolidation can be caused by repeated shaking events (Locat and Lee, 2002). The continuous magnetostratigraphic record at Unit I (Arculus et al., 2015a), however, excludes the existence of unconformities within the sequence, and it is unlikely that seismic events only caused overconsolidation of the interval of Unit I below 83 mbsf without also affecting the top of the section in this tectonically active region.

5.3.3. Compositional control

Compaction of sediments can be controlled by variations in the composition and size of sedimentary grains, with, for example, platy hyllosilicate minerals tending to facilitate compaction. However, no major change in phyllosilicate mineralogy, grain size or degree of bioturbation of the mudrocks of Unit I (Arculus et al., 2015a) corresponds with the sharp onset of fabric development at 83 mbsf. Curtis et al. (1980) have demonstrated that although preferred orientations in clay-rich sediments commonly result from compactional strain, fabric development may be affected by the presence of non-platy silicate particles (such as quartz grains) which inhibit planar fabric development in their immediate vicinity. In this context, we note a downhole decrease in the volume percentage of fine-grained quartz particles in the mudrocks, from an average of 8% to 4% (based on smear-slide data collected during shipboard analyses; Arculus et al., 2015a). This minor compositional change is illustrated semi-quantitatively by variations in the intensity of quartz peaks at 26.6° 2 θ in XRD

295 analyses of Unit I mud samples (Figure 2g; data from Arculus et al., 2015a).
296 Quartz content, however, mainly decreases between 50 and 65 mbsf (Figure 2g),
297 and remains constant throughout the interval where sharp variations of AMS
298 parameters are observed. Furthermore, the volume percentage change in quartz
299 affecting fabric development in the mudrocks analysed by Curtis et al. (1980)
300 was much more dramatic (28% to 15%). Finally, the combined volume
301 percentage of the main non-platy silicates (quartz plus feldspar) in Hole U1438B
302 increases slightly from 12% to 15% across the interval where AMS fabrics
303 develop (Arculus et al., 2015a), suggesting that this mechanism cannot account
304 for the stepwise change in anisotropy observed here.
305
306 *5.3.4. An effective stress threshold for the 'initial compaction window'*
307 The stepwise variation of anisotropy parameters, porosity/vertical shortening
308 and bulk density with depth documented here suggests that compaction and
309 sedimentary fabric development is not progressive, but only starts once the
310 burial load produces a sufficient effective stress to exceed the internal resistance
311 to compaction represented by the friction along grain contacts during
312 reorientation. In this case, the density data of Figure 2d, a water depth of 4700 m
313 and a seawater density of 1029 kg/m^3 combine to yield an effective stress at 83
314 mbsf of 0.35 MPa (where effective stress = total stress – pore water pressure
315 (assumed to be hydrostatic); Terzaghi, 1925). Sedimentary fabric in the studied
316 section then develops over a restricted interval between 83 and 113 mbsf here
317 defined as the 'initial compaction window', where pore reduction and preferred
318 horizontal alignment of phyllosilicate flakes is progressively enhanced over a 30
319 m-thick interval. A similar compaction window can also be inferred in pelagic

sediments from ODP Site 1149 in the NW Pacific Ocean, where a stepwise change in physical properties occurs between 118 and 150 mbsf (Kawamura and Ogawa, 2002; 2004).

5.4 Implications for fabric studies on deformed ancient mudrocks

The excellent age control at Site U1438, based on the IODP Expedition 351 shipboard magnetostratigraphy that successfully identified every geomagnetic chron in core sections back to 36 Ma (Arculus et al., 2015a), provides constraints on the timing of initial development of sedimentary fabrics in Unit I mudrocks. These indicate that the full process of fabric development documented here started 5.7 Ma after initial deposition and then took 6.5 Ma to complete (Figure 2e). This has implications for studies using AMS to document the progressive tectonic overprinting of sedimentary fabrics in ancient mudrocks (e.g., Sagnotti et al., 1998; Larrasoaña et al., 2004). Such studies typically assume that initial sedimentary fabrics (which are subsequently partially overprinted by tectonic fabrics) correspond to the biostratigraphic age of the sampled rocks. Instead results here suggest that a ~6 Ma hiatus between deposition and initial fabric development may need to be considered when documenting the evolution of anisotropy in deep marine mudrocks.

6. Conclusions

A detailed record of progressive fabric development in deep marine sediments sampled at IODP Site U1438 with robust age control indicates that a compaction-related horizontal foliation started to form 5.7 Ma after initial sedimentation (83 mbsf) and developed over the subsequent 6.5 Ma (down to 113 mbsf), within a

345 30 m-thick interval here termed the 'initial compaction window'. These new
346 results provide the first high-resolution time/depth constraints on the onset of
347 fabric development in deep marine environments, with implications for the
348 tectonic application of AMS in pelagic sedimentary rocks. More data are now
349 required from such deep marine environments to determine the variability in
350 the onset of the initial compaction window, including additional quantification of
351 clay microfabrics through this window using scanning electron microscope
352 (SEM) and transmission electron microscope (TEM) techniques.
353

354 **Acknowledgements**

355 This research used samples and data provided by International Ocean Discovery
356 Program (IODP). We thank the members of IODP expedition 351 Science Party
357 and the captain and crew of the JOIDES Resolution. Shipboard bulk density and
358 porosity measurements were performed by Mike Gurnis and Morihisa Hamada,
359 and the anisotropy of magnetic susceptibility measurements on discrete samples
360 by Matthew Meyer (Plymouth University).
361 Funding: This work was supported by the Natural Environment Research
362 Council [grant number NE/M007367/1 awarded to AM]; and the European
363 Research Council [grant number 306810, awarded to D.J.J. van Hinsbergen]. The
364 paper benefitted from thoughtful reviews by Eric Ferré and an anonymous
365 reviewer.
366

367 **References**

368 Acton, G. D., 2002. Paleomagnetic overprints in ocean sediment cores and their
369 relationship to shear deformation caused by piston coring. J. Geophys. Res.
370 107, doi: 10.1029/2001JB000518.

371 Anson, G. L. and Kodama, K. P., 1987. Compaction-induced inclination shallowing
372 of the post-depositional remanent magnetization in a synthetic sediment.
373 Geophys. J. Int. 88, 673-692.
374 Arason, P. and Levi, S., 1990. Compaction and inclination shallowing in deep-sea
375 sediments from the Pacific Ocean, J. Geophys. Res., 95(B4), 4501-4510,
376 doi:10.1029/JB095iB04p04501.
377 Arculus, R. J., Ishizuka, O., Bogus, K. and the Expedition 351 Scientists, 2015a.
378 Proceedings of the International Ocean Discovery Program Volume 351,
379 doi:10.14379/iodp.proc.351.103.2015.
380 Arculus, R. J., Ishizuka, O., Bogus, K., Gurnis, M., Hickey-Vargas, R., Aljahdali, M. H.,
381 Bandini-Maeder, A. N., Barth, A. P., Brandl, P., Drab, L., do Monte Guerra, R.,
382 Hamada, M., Jiang, F., Kanayama, K., Kender, S., Kusano, Y., Li, H., Loudin, L.
383 C., Maffione, M., Marsaglia, K. M., McCarthy, A., Meffre, S., Morris, A., Neuhaus,
384 M., Savov, I. P., Sena, C., Tepley III, F. J., van der Land, C., Yogodzinski, G. M.
385 and Zhang, Z., 2015b. A record of spontaneous subduction initiation in the
386 Izu–Bonin–Mariana arc. Nat. Geosci. 8, 728–733, doi: 10.1038/ngeo2515.
387 Athy, L. F., 1930. Density, porosity and compaction of sedimentary rocks
388 (abstract). American Association of Petroleum Geologists, Bulletin, 14, 24.
389 Bennett, R. H., Bryant, W. R. and Keller, G. H., 1981. Clay fabric of selected
390 submarine sediments: fundamental properties and models. J. Sediment.
391 Petrol. 51, 217-232.
392 Bennett, R. H., O'Brien, N. R. and Hulbert, M. H., 1991. Determinants of clay and
393 shale microfabric signatures: processes and mechanisms. In: Bennett, R. H.,
394 Bryant, W. R. and Hulbert, M. H. (Eds.), Microstructures of Fine-grained
395 Sediments from Mud to Shale. Springer-Verlag, New York, pp. 5 –32.
396 Bennett, R. H. and Hulbert, M. H., 1986. Clay Microstructure. Boston
397 (International Human Resources Development Corp. Publ.).
398 Bjørlykke, K. and Høeg, K., 1997. Effects of burial diagenesis on stresses,
399 compaction and fluid flow in sedimentary basins. Marine and Petroleum
400 Geology, 14**,** 267-276.
401 Borradaile, G. J., 1988. Magnetic-susceptibility, petrofabrics and strain:
402 Tectonophysics 156, 1–20, doi: 10.1016/0040-1951(88)90279-x.
403 Borradaile, G. J. and Jackson, M., 2004. Anisotropy of magnetic susceptibility
404 (AMS): magnetic petrofabrics of deformed rocks. Geol. Soc. London Sp. Pub.
405 238, 299–360, doi: 10.1144/GSL.SP.2004.238.01.18.
406 Burmeister, K. C., Harrison, M. J., Marshak, S., Ferré, E. C., Bannister, R. A. and
407 Kodama, K. P., 2009. Comparison of Fry strain ellipse and AMS ellipsoid
408 trends to tectonic fabric trends in very low-strain sandstone of the
409 Appalachian fold–thrust belt. J. Struct. Geol. 31, 1028-1038.
410 Curtis, C. D., Lipshie, S. R., Oertel, G. and Pearson, M. J., 1980. Clay orientation in
411 some Upper Carboniferous mudrocks, its relationship to quartz content
412 and some inferences about fissility, porosity and compactional history.
413 Sedimentology 27, 333-339.
414 Deschamps, A. and Lallemand, S., 2003. Geodynamic setting of Izu-Bonin-
415 Mariana boninites. Geol. Soc. London Sp. Publ. 219, 163–185, doi:
416 10.1144/GSL.SP.2003.219.01.08.
417 Dunlop, D. J. and Özdemir, Ö., 1997. Rock magnetism: fundamentals and
418 frontiers. Cambridge University Press, Cambridge, 573 pp.
419 Hamilton, E. L., 1976. Variations of density and porosity with depth in deep sea

sediments. Journal of Sedimentary Petrology, 46, 280-300.
Hirano, S., Ogawa, Y. and Kawamura, K., 2001. Deformation of unlithified sediments in an early stage of the compaction process deduced from microtextures and magnetic fabrics: ODP Leg 174B, Hole 1074A. In: Becker, K., Malone, M.J. (Eds.), Proc. ODPSci. Results, vol. 174B, 1 –13.
Hrouda, F., 1982. Magnetic anisotropy of rocks and its application in geology and geophysics. Geophys. Surveys 5, 37–82, doi: 10.1007/BF01450244.
Hrouda, F. and Jezek, J., 1999. Magnetic anisotropy indications of deformations associated with diagenesis. In: Tarling, D. H. and Turner, P. (eds), Palaeomagnetism and Diagenesis in Sediments, Geological Society, London, Special Publication, 151, 127-137.
Huang, W., Dupont-Nivet, G., Lippert, P. C., van Hinsbergen, D. J. J. and Hallot, E., 2013. Inclination shallowing in the Eocene Linzizong sediments from Tibet: correction, possible causes and implications for reconstructing the India-Asia collision. Geophys. J. Int. 194, 1390-1411.
Ishizuka, O., Taylor, R. N., Yuasa, M. and Ohara, Y., 2011a. Making and breaking an island arc: A new perspective from the Oligocene Kyushu-Palau arc, Philippine Sea. Geochem. Geophys. Geosys. 12, 1–40, doi: 10.1029/2010GC003440.
Ishizuka, O., Tani, K., Reagan, M. K., Kanayama, K., Umino, S., Harigane, Y., Sakamoto, I., Miyajima, Y., Yuasa, M. and Dunkley, D. J., 2011b. The timescales of subduction initiation and subsequent evolution of an oceanic island arc. Earth Planet. Sci. Lett. 306, 229–240, doi: 10.1016/j.epsl.2011.04.006
Ishizuka, O., Taylor, R. N., Ohara, Y. and Yuasa, M. , 2013. Upwelling, rifting, and age-progressive magmatism from the Oki-Daito mantle plume. Geology, 41, 1011–1014.
Jelínek, V., 1978. Statistical processing of anisotropy of magnetic susceptibility measured on groups of specimens. Studia Geophys. Geod. 22, 50–62, doi: 10.1007/BF01613632.
Jelínek, V., 1981. Characterization of the magnetic fabric of rocks. Tectonophysics 79, 63-67.
Johnson, C. L., Constable, C. G., Tauxe, L., Barendregt, R., Brown, L. L., Coe, R. S., Layer, P., Mejia, V., Opdyke, N. D., Singer, B. S., Staudigel, H. and Stone, D. B., 2008. Recent investigations of the 0-5 Ma geomagnetic field recorded by lava flows. Geochemistry, Geophys. Geosystems, *9*(4), doi:10.1029/2007GC001696.
Kawamura, K. and Ogawa, Y., 2002. Progressive microfabric changes in unconsolidated pelagic and hemipelagic sediments down to 180 mbsf, northwest Pacific, ODP Leg 185, Site 1149. In Ludden, J.N., Plank, T., and Escutia, C. (Eds.), Proc. ODP, Sci. Results, 185.
Kawamura, K. and Ogawa, Y., 2004. Progressive change of pelagic clay microstructure during burial process: examples from piston cores and ODP cores. Marine Geol. 207, 131-144. doi:10.1016/j.margeo.2004.03.016.
Kopf, A. and Behrmann, J. H., 1997. Fabric evolution and mechanisms of diagenesis in fine-grained sediments from the Kita-Yamato Trough, Japan Sea. J. Sedim. Res. 67, 590–600.
Larrasoaña, J. C., Pueyo, E. L. and Pares, J. M., 2004. An integrated AMS, structural, palaeo- and rock-magnetic study of Eocene marine marls from the Jaca-

469 Pamplona basin (Pyrenees, N Spain); new insights into the timing of
470 magnetic fabric acquisition in weakly deformed mudrocks. Geol. Soc.
471 London Sp. Publ. 238, 127–143, doi: 10.1144/GSL.SP.2004.238.01.10.
472 Locat, J. and Lee, H., 2002. Submarine landslides: Advances and challenges.
473 Canadian Geotech. J. 39, 193–212.
474 Maffione, M., Pucci, S., Sagnotti, L. and Speranza, F., 2012. Magnetic fabric of
475 Pleistocene continental clays from the hanging-wall of an active low-angle
476 normal fault (Altotiberina Fault, Italy). Int. J. Earth Sci. 101, 849–861, doi:
477 10.1007/s00531-011-0704-9.
478 Maffione, M., Hernandez-Moreno, C., Ghiglione, M. C., Speranza, F., van
479 Hinsbergen, D. J. J. and Lodolo, E., 2015. Constraints on deformation of the
480 Southern Andes since the Cretaceous from anisotropy of magnetic
481 susceptibility. Tectonophysics 665, 236–250, doi:
482 10.1016/j.tecto.2015.10.008.
483 Mondol, N. H., Fawad, M., Jahren, J. and Bjørlykke, K.,, 2008. Synthetic mudstone
484 compaction trends and their use in pore pressure prediction. First Break,
485 26, 43-51.
486 Okino, K. and Fujioka, K., 2003. Central basin spreading center, Philippine Sea:
487 Structure of an extinct spreading center and implications for marginal basin
488 information. J. Geophys. Res. 108, 2040, doi:10.1029/2001JB001095.
489 Okino, Y., Shimakawa, Y. and Nagaoka, S., 1994. Evolution of the Shikoku Basin. J.
490 Geomag. Geoelect. 46, 463–479.
491 Parés, J. M., 2015. Sixty years of anisotropy of magnetic susceptibility in
492 deformed sedimentary rocks. Frontiers Earth Sci. 3, 1–13, doi:
493 10.3389/feart.2015.00004.
494 Potter, D. K. and Stephenson, A., 1988. Single-domain particles in rocks and
495 magnetic fabric analysis. Geophysical Research Letters, 15, 1097-1100, doi:
496 10.1029/GL015i010p01097.
497 Reagan, M. K., Ishizuka, O., Stern, R. J., Kelley, K. A., Ohara, Y., Blichert-Toft, J.,
498 Bloomer, S. H., Cash, J., Fryer, P., Hanan, B. B., Hickey-Vargas, R., Ishii, T.,
499 Kimura, J. I., Peate, D. W., Rowe, M. C. and Woods, M., 2010. Fore-arc basalts
500 and subduction initiation in the Izu-Bonin-Mariana system. Geochem.
501 Geophys. Geosys., 11, 1–17, doi: 10.1029/2009GC002871.
502 Reynolds, S. and Gorsline, D.S., 1992. Clay microfabrics of deep sea mud(stones),
503 California Continental Borderland. J. Sed. Petr. 62, 41-53.
504 Rochette, P., Jackson, M. and Aubourg, C., 1992. Rock Magnetism and the
505 interpretation of magnetic susceptibility. Reviews Geophys. 30, 209–226.
506 Sagnotti, L. and Speranza, F., 1993. Magnetic fabric analysis of the Plio-
507 Pleistocene clayey units of the Sant'Arcangelo basin, southern Italy. Physics
508 of the Earth and Planetary Interiors, 77, 165-176.
509 Sagnotti, L., Speranza, F., Winkler, A., Mattei, M. and Funiciello, R., 1998. Magnetic
510 fabric of clay sediments from the external northern Apennines (Italy). Phys.
511 Earth Planet. Int. 105, 73–93, doi: 10.1016/S0031-9201(97)00071-X.
512 Schwehr, K., Tauxe, L., Driscoll, N. and Lee, H., 2006. Detecting compaction
513 disequilibrium with anisotropy of magnetic susceptibility. Geochem.
514 Geophys. Geosys. 7, doi: 10.1029/2006GC001378.
515 Schlater, J. G. and Christie, P. A. F., 1980. Continental stretching: an explanation of
516 the post-mid-Cretaceous subsidence of the Central North Sea basin. Journal
517 of Geophysical Research, 85, 3711-3739.

518 Tarling, D. and Hrouda, F. (Eds.), 1993. Magnetic anisotropy of rocks. Springer
519 Science & Business Media.
520 Tauxe, L. and Kent, D. V., 2004. A simplified statistical model for the geomagnetic
521 field and the detection of shallow bias in paleomagnetic inclinations: was
522 the ancient magnetic field dipolar? Timescales Paleomag. Field, 145, 101–
523 115.
524 Terzaghi, K., 1925. Erdbaumechanik auf Bodenphysikalischer Grundlage. Franz
525 Deuticke, Liepzig-Vienna, 274 p.
526
527

528 **Figure captions**
529
530 Figure 1. (a) Location map of the Philippine Sea Plate (PSP) showing the main
531 geological structures and domains inferred from bathymetry, and the location of
532 IODP Site U1438. (b) Lithostratigraphic log from Site U1438. The grain size is
533 averaged over 5 m thick intervals. (cl) clay; (si) silt; (vfs-fs) very fine to fine sand;
534 (ms-vcs) medium to very coarse sand; (gr), granules. Unit subdivision is
535 indicated.
536
537 Figure 2. (a-c) Anisotropy of magnetic susceptibility results from 173 discrete
538 cubic samples from Unit I, IODP Hole U1438B, showing the variation with depth
539 of (a) the corrected anisotropy degree, P_J (b) the shape parameter, T, and (c)
540 mean susceptibility. (d-g) Variation with depth of physical property and
541 lithostratigraphic data from IODP Expedition 351 shipboard measurements
542 (Arculus et al., 2015a). (d) Density and porosity data from discrete samples. (e)
543 Age model based on magnetostratigraphy. Each point on the age-depth curve
544 represents a reversal of the magnetic polarity in the core dated using the
545 reference geomagnetic polarity time scale (GPTS). Sedimentation rates are
546 calculated on the basis of the magnetostratigraphy. (f) Simplified
547 lithostratigraphic log of Unit I. (g) Proxy for quartz content derived from peak
548 intensities on X-Ray diffraction spectra (note arbitrary units). The two dotted
549 gray lines bracket the interval in which anisotropy and physical parameters
550 progressively change (here defined as the 'initial compaction window').
551
552 Figure 3. Stereographic equal area projections of the principal susceptibility axes
553 from samples (a) above and (b) below 83 mbsf.
554
555 Figure 4. (a) High-temperature variation of low-field magnetic susceptibility
556 during a complete heating-cooling cycle, showing a clear Curie temperature of
557 ~580°C (heating curve). The cooling curve shows a slightly higher Curie
558 temperature probably due to the oxidation of original magnetite to maghemite.
559 (b) Isothermal remanent magnetization (IRM) acquisition curve from a
560 representative sample showing presence of low coercivity magnetite. (c)
561 Susceptibility vs. intensity of natural remanent magnetization (NRM) showing a
562 linear relationship suggesting constancy of ferromagnetic mineralogy downhole.
563
564 Figure 5. Variation with depth of (a) inclination and (b) declination of the
565 magnetic remanence in Unit I after alternating field (AF) demagnetization at 25

mT of archive half core sections (2 cm measurement interval; see Arculus et al. (2015b) for full description of methodology). Data are in geographic coordinates, after correction using FlexIT core orientation tool data. Declination and inclination vary downward due to the reversals of the geomagnetic field. (a) Inclination decreases significantly below core 9H (the effect is more visible in the normally magnetized intervals). (b) Declination varies within each core likely due to drilling-induced shear effects, particularly evident in cores 3H, 5H, 8H, and 13H. The shear effect is expected to be minimum at the bottom of each core. (c) Core distribution with depth from Hole U1438B.

Figure 6. Representative orthogonal vector plots of demagnetization data from intervals used for the calculation of the mean inclination. We select only those intervals in which 25 mT AF steps provide a reliable measure of the isolated characteristic remanent magnetization directions (i.e., declination and inclination of the 25 mT step is at an angle < 10° from the best fit line calculated using the 20-40 mT interval). Black (white) dots represent the declination (inclination) projection.

Figure 7. Variation of uniaxial vertical shortening derived from the density data of Figure 2d (open circles) compared to published theoretical compaction trends for clays and claystones. The two dotted gray lines bracket the interval in which anisotropy and physical parameters progressively change (here defined as the 'initial compaction window').

Table S1. Summary of anisotropy of magnetic susceptibility data from Unit I of IODP Hole U1438B.

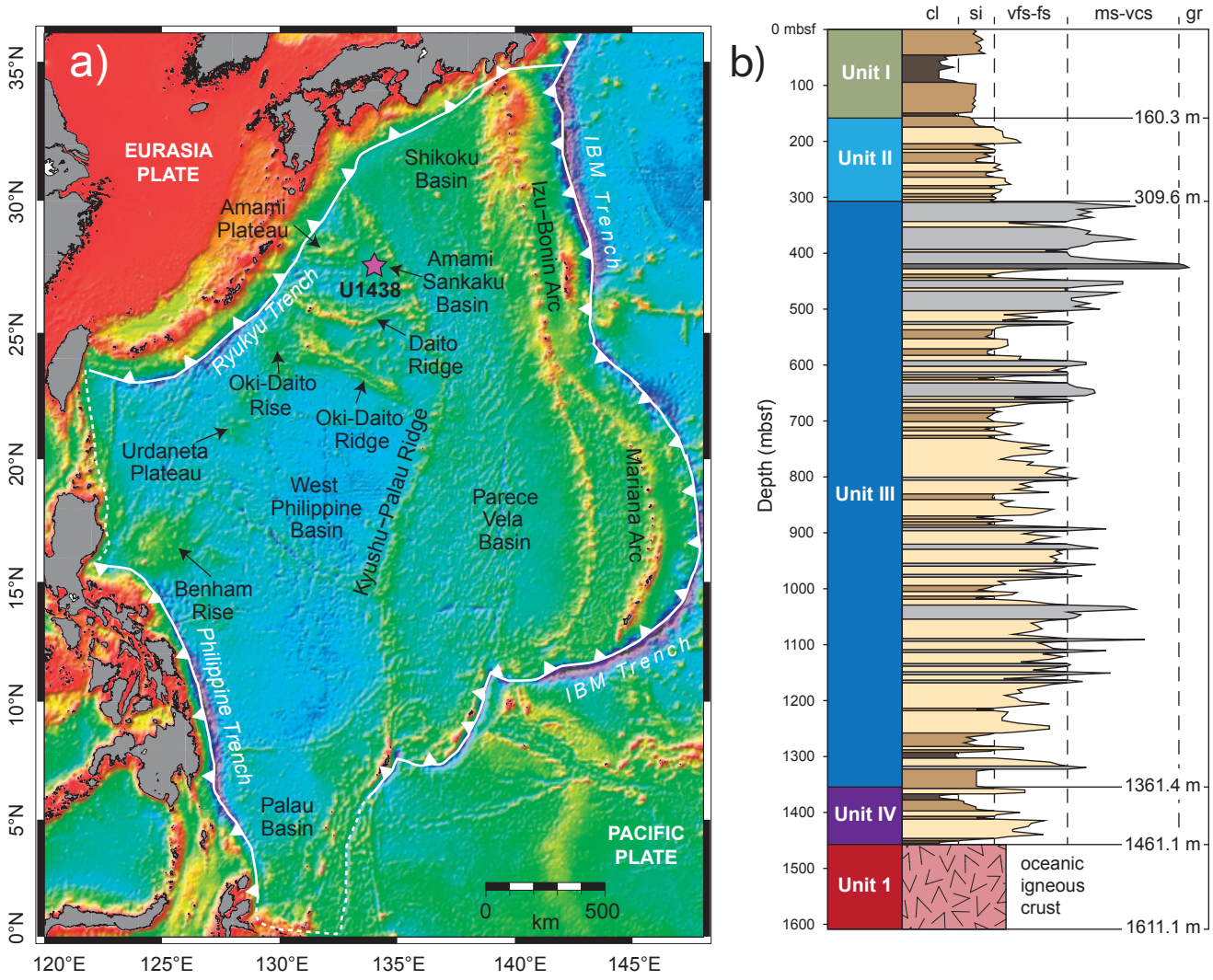
a)
EURASIA PLATE
PACIFIC PLATE
Shikoku Basin
Amami Plateau
Amami Sankaku Basin
U1438
Izu-Bonin Arc
IBM Trench
Ryukyu Trench
Daito Ridge
Oki-Daito Rise
Oki-Daito Ridge
Urdaneta Plateau
West Philippine Basin
Kyushu-Palau Ridge
Parece Vela Basin
Mariana Arc
Benham Rise
Philippine Trench
Palau Basin
IBM Trench
0 km 500
35°N
30°N
25°N
20°N
15°N
10°N
5°N
0°N
120°E
125°E
130°E
135°E
140°E
145°E
b)
cl
si
vfs-fs
ms-vcs
gr
0 mbsf
Depth (mbsf)
Unit I
Unit II
Unit III
Unit IV
Unit 1
160.3 m
309.6 m
1361.4 m
1461.1 m
1611.1 m
oceanic igneous crust

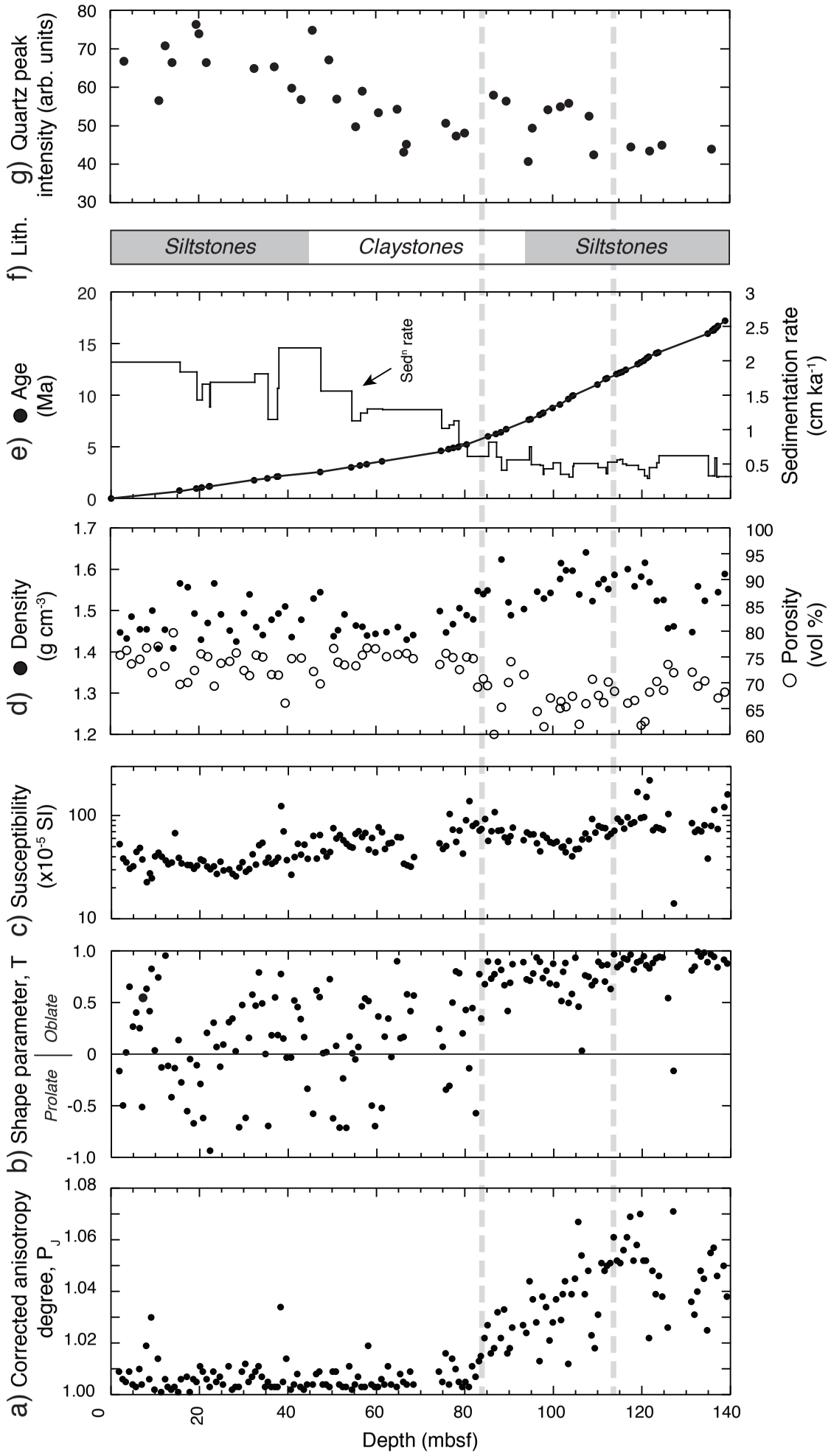
g) Quartz peak intensity (arb. units)
f) Lith.
Siltstones
Claystones
Siltstones
e) ● Age (Ma)
Sedⁿ rate
Sedimentation rate (cm ka⁻¹)
d) ● Density (g cm⁻³)
○ Porosity (vol %)
c) Susceptibility (x10⁻⁵ SI)
b) Shape parameter, T
Oblate
Prolate
a) Corrected anisotropy degree, P_J
Depth (mbsf)

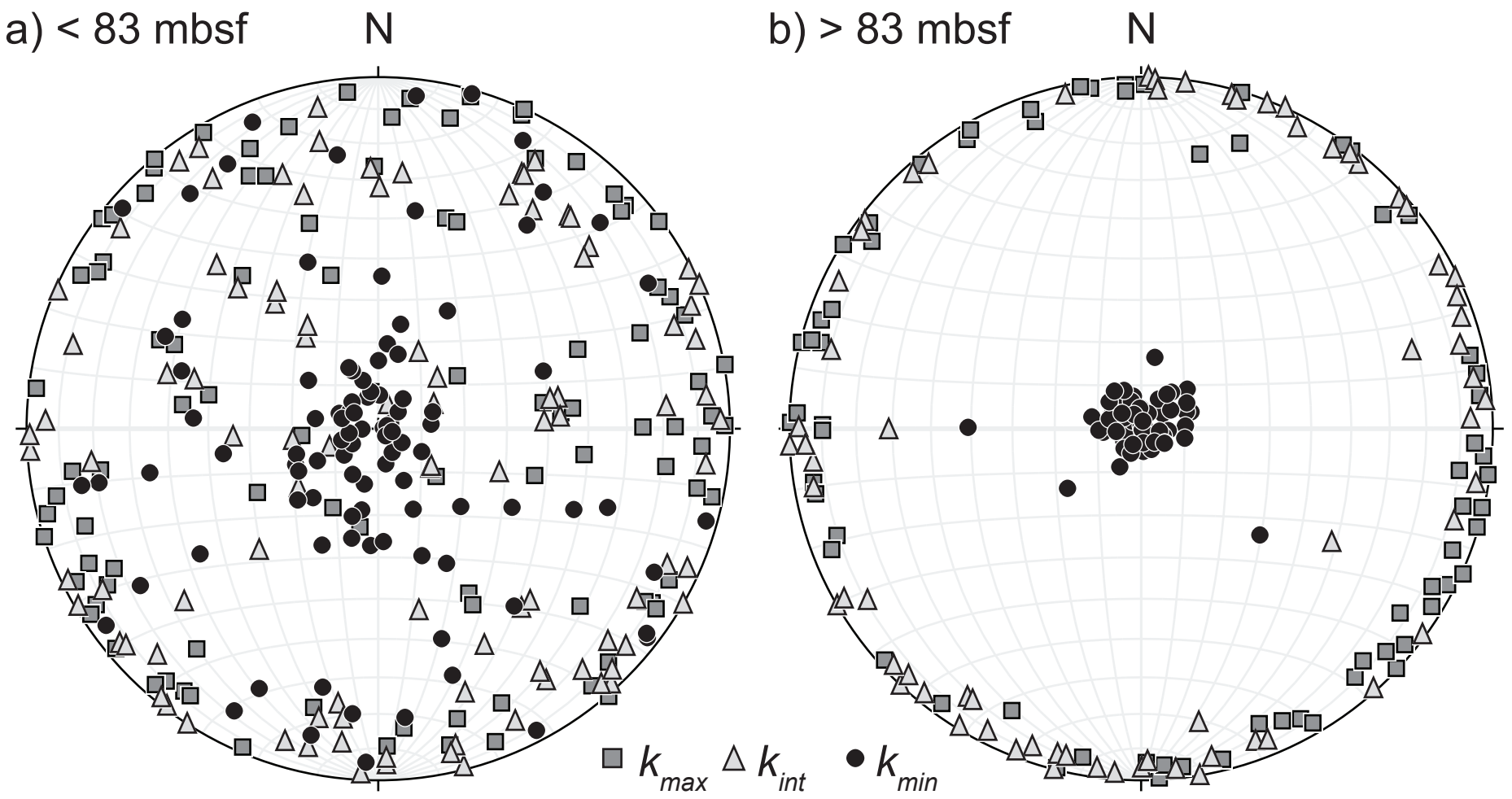
a) < 83 mbsf
N
b) > 83 mbsf
N
k_{max}
k_{int}
k_{min}

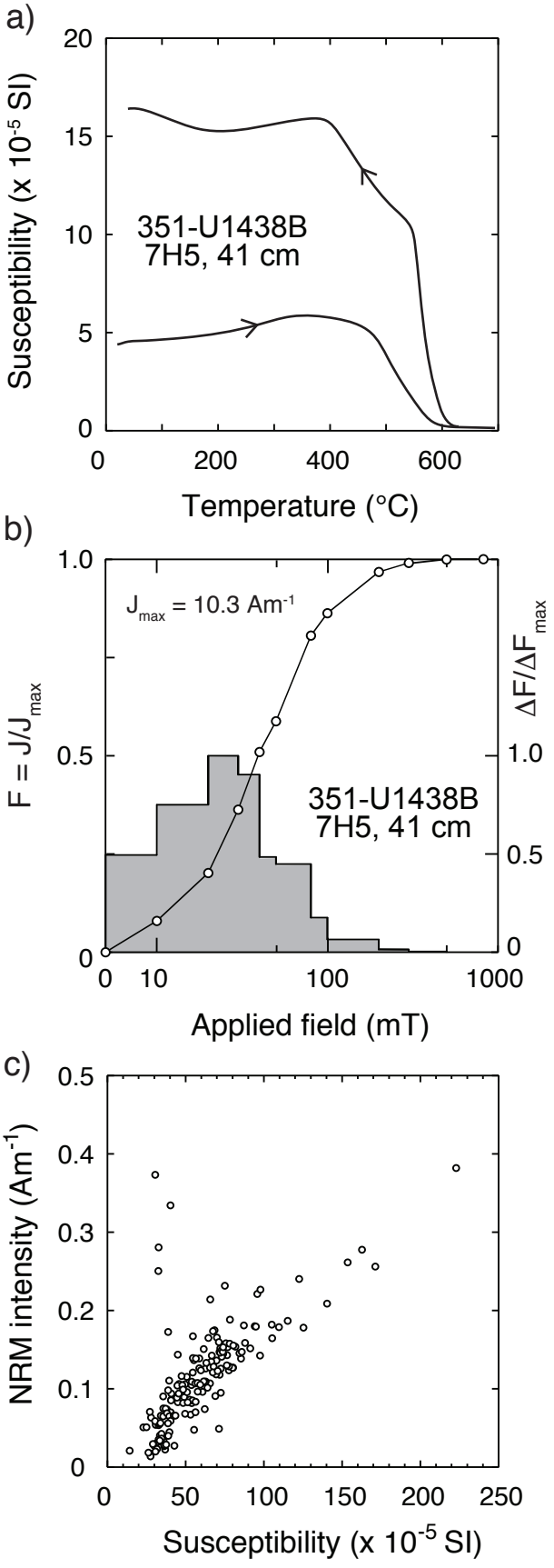
a)
Susceptibility (x 10-5 SI)
20
15
10
5
0
351-U1438B
7H5, 41 cm
0
200
400
600
Temperature (°C)
b)
1.0
0.5
0
F = J/Jmax
Jmax = 10.3 Am-1
351-U1438B
7H5, 41 cm
ΔF/ΔFmax
1.0
0.5
0
0
10
100
1000
Applied field (mT)
c)
NRM intensity (Am-1)
0.5
0.4
0.3
0.2
0.1
0
0
50
100
150
200
250
Susceptibility (x 10-5 SI)

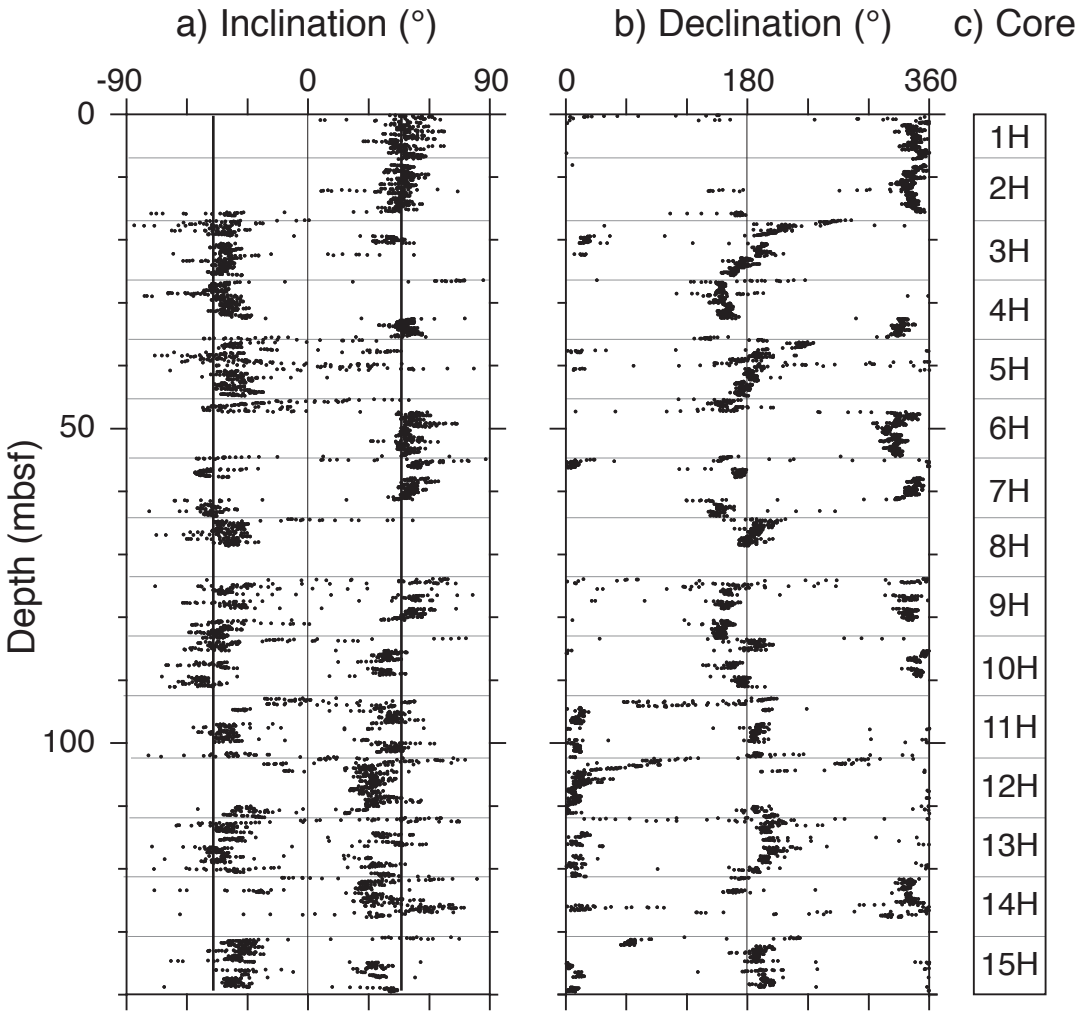
a) Inclination (°)
b) Declination (°)
c) Core
-90
0
90
0
180
360
Depth (mbsf)
0
50
100
1H
2H
3H
4H
5H
6H
7H
8H
9H
10H
11H
12H
13H
14H
15H

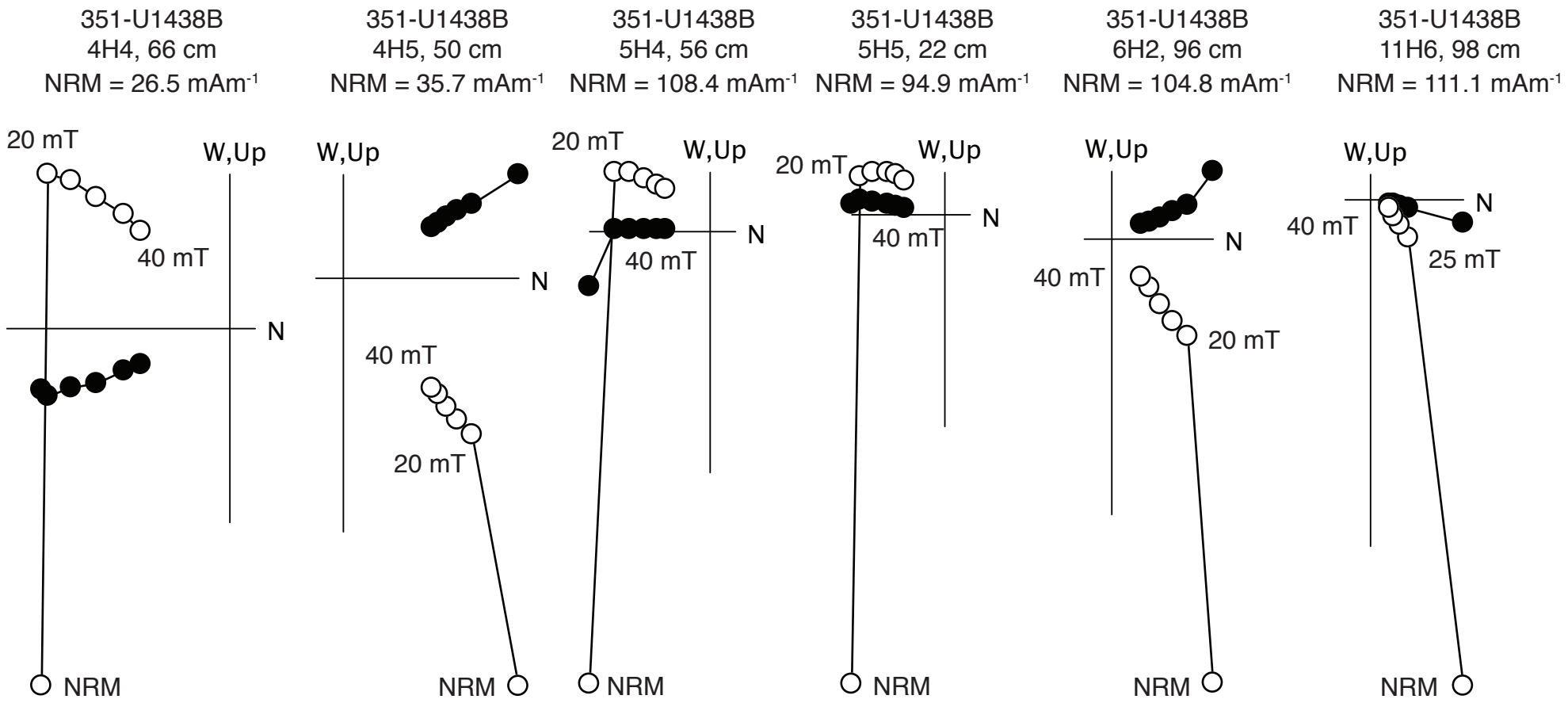
351-U1438B
4H4, 66 cm
NRM = 26.5 mAm-1
20 mT
W,Up
40 mT
N
NRM
351-U1438B
4H5, 50 cm
NRM = 35.7 mAm-1
W,Up
N
40 mT
20 mT
NRM
351-U1438B
5H4, 56 cm
NRM = 108.4 mAm-1
20 mT
W,Up
N
40 mT
NRM
351-U1438B
5H5, 22 cm
NRM = 94.9 mAm-1
20 mT
W,Up
N
40 mT
NRM
351-U1438B
6H2, 96 cm
NRM = 104.8 mAm-1
W,Up
N
40 mT
20 mT
NRM
351-U1438B
11H6, 98 cm
NRM = 111.1 mAm-1
W,Up
N
40 mT
25 mT
NRM

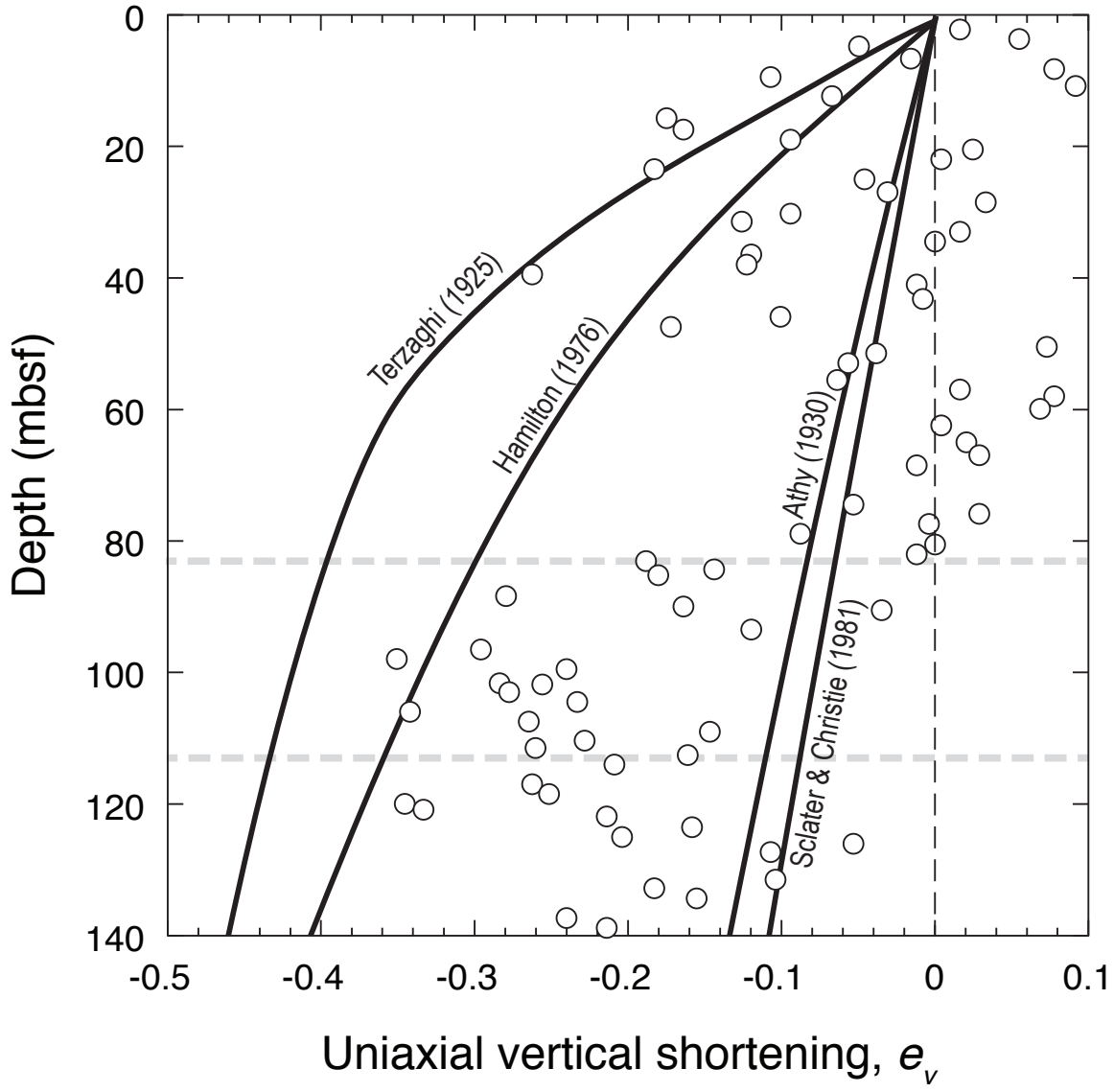
Depth (mbsf)
0
20
40
60
80
100
120
140
-0.5
-0.4
-0.3
-0.2
-0.1
0
0.1
Uniaxial vertical shortening, e_v
Terzaghi (1925)
Hamilton (1976)
Athy (1930)
Sclater & Christie (1981)